

# Coordination and Haptotropic Migration of Cr(CO)<sub>3</sub> in Polycyclic Aromatic Hydrocarbons: The Effect of the Size and the Curvature of the Substrate

J. Oscar C. Jiménez-Halla,<sup>†</sup> Juvencio Robles,<sup>‡</sup> and Miquel Solà\*<sup>†</sup>

*Institut de Química Computacional and Departament de Química, Universitat de Girona, Campus de Montilivi, 17071 Girona, Catalonia, Spain, and Facultad de Química, Universidad de Guanajuato, Noria Alta s/n 36050 Guanajuato, Gto. Mexico*

*Received: September 19, 2007; In Final Form: November 16, 2007*

In this work, we study the reaction mechanism of the tricarbonylchromium complex haptotropic rearrangement between two six-membered rings arranged like in naphthalene of four polycyclic aromatic hydrocarbons (PAHs). It has been found that the reaction mechanism of this haptotropic migration can either occur in a single step or stepwise depending on the interaction between the orbitals of the Cr(CO)<sub>3</sub> and the PAH fragments. Our results show that the size of the cyclic system favors the metal migration whereas the curvature of the organic substrate tends to slow down the rearrangement. We discuss the key factors that help to explain this behavior through orbital and energy decomposition analysis.

## 1. Introduction

One of the first characteristics discovered in  $\pi$ -coordinated metal complexes, such as the tricarbonylchromium complex coordinated to polycyclic aromatic hydrocarbons (PAHs), was their ability to undergo thermal  $\eta^6, \eta^6$ -inter-ring haptotropic rearrangements (IRHR) in which the  $\pi$ -coordinated metal migrates between different rings of the PAH.<sup>1–3</sup> The simplest system where an IRHR takes place is in the ( $\eta^6$ -naphthalene)-Cr(CO)<sub>3</sub> complex and their derivatives. For these species, mechanistic studies were performed to discern the nature of  $\pi$ -coordinated metal binding.<sup>4–6</sup> It was found that the interactions between low-lying unoccupied orbitals of Cr(CO)<sub>3</sub> and high-lying occupied  $\pi$ -orbitals of naphthalene represent the dominant bonding mechanism, the tricarbonylchromium acting in these complexes as a powerful electron withdrawing group.<sup>7</sup>

This kind of reaction offers a plethora of possibilities in organic synthesis. Haptotropic shifts play an important role in reactions with electronically saturated complexes<sup>8–11</sup> and associative substitution reactions.<sup>12,13</sup> Remarkably, Dötz and co-workers have designed stereospecific molecular switches based on a reversible thermo- and photoinduced haptotropic shifts of the Cr(CO)<sub>3</sub> fragment along a naphthohydroquinone skeleton.<sup>2,14,15</sup> Some other important contributions addressed the topic of the diastereoselectivity in this reaction mechanism.<sup>12,15–17</sup> Recently, the selective migration of the Cr(CO)<sub>3</sub> group between two heterocyclic and phenyl neighboring rings through a combination of thermal and acid/base changes on the course of the reaction was reported.<sup>11</sup>

Coordination of the Cr(CO)<sub>3</sub> complex to a given PAH takes place usually to the ring with the highest electron density,<sup>8,18</sup> which is in many cases the least substituted ring and the most aromatic.<sup>8,16,19–21</sup> It is widely accepted that the structure, reactivity, and aromaticity of the PAH are altered significantly upon complexation with the tricarbonylchromium complex.

Thus, after complexation, the coordinated ring expands, loses its planarity, and shows an increased difference between alternated short and long C–C bonds.<sup>3,8</sup> Moreover, the reactivity of the coordinated ring changes dramatically due to complexation. The strong electron withdrawing character of the chromium tricarbonyl complex makes the coordinated PAH more susceptible to nucleophilic addition rather than electrophilic substitution and also increases the acidity of the aryl and benzylic hydrogens.<sup>3,7,22</sup> Interestingly, haptotropic migrations are found to obey first-order kinetics suggesting that migration occurs through intramolecular metal shifts.<sup>15,16,23</sup> The intrinsic energy barrier associated to this haptotropic migrations depends on the substrate and can vary from about 20 to 50 kcal·mol<sup>-1</sup>, as it has been reported by several authors.<sup>10,14–16,23–26</sup>

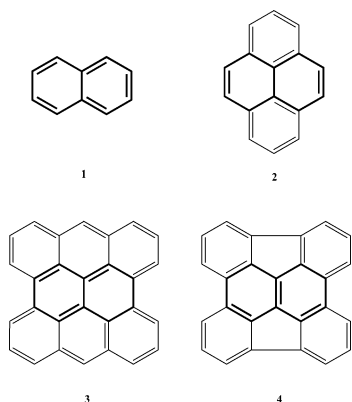
Some earlier theoretical studies based on extended Hückel calculations scanned the potential energy surface (PES) searching for the minimal energy path for which these haptotropic migrations take place.<sup>4,27</sup> As it was reported, the metal prefers to move along the  $\pi$ -plane in the periphery of the system of rings rather than follow the least motion path from the center of one ring to the center of the second ring through the middle of the C–C bond common to the two adjacent rings. In other words, the system evolves through  $\eta^6 \rightarrow \eta^1 \rightarrow \eta^6$  coordination states (or even  $\eta^6 \rightarrow \eta^3 \rightarrow \eta^6$ ) instead of  $\eta^2$ -transition states (TSs) because the overlapping between *d*-filled orbitals of the metal center and  $\pi$ -orbitals of the PAH part is favored in the first case. More recent density functional theory (DFT) and correlated ab initio studies in different substrates including nanotubes have confirmed the earlier results.<sup>10,11,16,26,28,29</sup>

An interesting experimental finding that has been confirmed theoretically is that the arene-Cr(CO)<sub>3</sub>  $\pi$ -interactions are less stabilizing as the size of the organic part becomes larger (for instance, along the series benzene  $\gg$  naphthalene  $>$  pyrene).<sup>16,27,30</sup> At the same time, the energy barrier for the haptotropic migration decreases when the size of the PAH increases.<sup>12,14–16,23</sup> A first aim of this paper is to confirm this result by analyzing the haptotropic migration in a series of three PAHs (**1–3** in Scheme 1) of different size sharing a common naphthalenic skeleton that (i) possess a central C–C bond with the same

\* Corresponding author. Tel: +34.972.41.89.12. Fax: +34.972.41.83.56. E-mail: miquel.sola@udg.es.

<sup>†</sup> Universitat de Girona.

<sup>‡</sup> Universidad de Guanajuato.

**SCHEME 1: Four Polycyclic Aromatic Hydrocarbons Studied in This Work<sup>a</sup>**


<sup>a</sup> The rings involved in the haptotropic rearrangement are depicted with a thicker line.

characteristics as that in naphthalene and (ii) have structural symmetry with respect to this central C–C bond. In these systems the rearrangement is thermoneutral since reactants and products are the same species. We are aware that the most stable ( $\eta^6$ -pyrene)Cr(CO)<sub>3</sub> is not the one we study but the one having the Cr(CO)<sub>3</sub> group coordinated to the outer ring of pyrene. However, our aim is not to study the most favorable experimental species but to analyze the equivalent haptotropic rearrangement in systems of increased size.

Another factor contributing to modify the energy barriers is the curvature of the organic fragment. For instance, it has been experimentally found that helical distortion of the PAH favors the metal shift. In addition, it is well-known that there are no complexes in which a metal coordinates in an  $\eta^6$ -fashion to a six-membered ring (6-MR) of C<sub>60</sub>.<sup>31</sup> Many theoretical studies have analyzed coordination and reactivity in curved PAHs like corannulene,<sup>20,32</sup> buckybowl,<sup>33,34</sup> fullerenes,<sup>35</sup> or even nanotubes.<sup>28</sup> However, to our knowledge, the IRHR in a curved PAH has never been compared with a planar reference system of the same or similar size to discuss the effect of the PAH curvature. In this work, we compare the stability and the energy barriers for haptotropic migration of the ( $\eta^6$ -PAH)tricarbonylchromium complexes **3** and **4** (Scheme 1) having almost the same size and different curvature with the aim to get a deeper insight into the effect of the curvature in haptotropic rearrangements.

Finally, we will briefly address the effect of tricarbonylchromium complexation on the aromaticity of the studied PAHs. Such an effect is rather controversial. According to Mitchell and co-workers,<sup>19,36</sup> the benzene ring in tricarbonylchromium-complexed benzene is about 30–40% more aromatic than benzene itself. Schleyer et al.<sup>37</sup> using nucleus-independent chemical shifts (NICS) and <sup>1</sup>H NMR chemical shifts data found that the aromaticity of the benzene ring in ( $\eta^6$ -C<sub>6</sub>H<sub>6</sub>)Cr(CO)<sub>3</sub> is similar to that of the free benzene molecule. On the other hand, Simion and Sorensen<sup>38</sup> concluded from diamagnetic susceptibility exaltation data that the benzene ring coordinated to the chromium tricarbonyl complex is antiaromatic. A similar opinion is held by Hubig et al.,<sup>3</sup> who consider that the charge transfer from the arene to the transition metal in metal–arene coordination leads to a complete loss of aromaticity of the  $\pi$ -system. We have recently shown by means of different indicators of aromaticity that there is an important reduction of the aromaticity of benzene when coordinated to Cr(CO)<sub>3</sub>.<sup>39</sup> In this paper, we will use the structural (HOMA) and electronic

(PDI, FLU) indices for measuring quantitatively the changes in aromaticity induced by coordination of Cr(CO)<sub>3</sub> to the studied PAHs.

**2. Computational Details**

Geometry optimizations were computed with Gaussian 03<sup>40</sup> by means of the nonlocal three-parameter Becke's exchange functional<sup>41</sup> and the gradient-corrected Lee–Yang–Parr correlation functional,<sup>42</sup> classically known as B3LYP. It has been shown that the species involved in the haptotropic migration have single reference character, and therefore, a method such as B3LYP is adequate for this study.<sup>16</sup> The addition of polarization functions have been shown to be important to correctly describe the Cr–arene interaction in these kind of complexes.<sup>43</sup> Consequently, we employed a polarized mixed basis set: 6-31G(d,p)<sup>44</sup> for C, O, and H atoms and for the chromium atom we utilized a Wachters-type basis set with polarization functions:<sup>45</sup> (14s9p5d3f)/(8s4p3d1f) using the expanded contraction scheme (62111111/3312/311/3). Relativistic effects are unimportant for accurate calculations of chromium complexes<sup>46</sup> and were neglected in our calculations. Finally, since actual experiments are typically carried out in rather unipolar solvents, solvent effects are small<sup>29</sup> and have not been considered in our study. All species described throughout the paper are closed-shell singlets that have been treated using the restricted formalism.

Critical points on PES were characterized by the correct number of negative eigenvalues computing harmonic vibrational frequencies; this number must be zero for minima and one for any true transition state (TS). We also verified that the imaginary frequency exhibits the expected motion. Energy was corrected by adding the zero-point energy (ZPE) and the basis set superposition error (BSSE) in the critical points of the PES according to the following expression:

$$\Delta E = \Delta E_{\text{el}} + \text{ZPE}(\text{AB}) - \text{ZPE}(\text{A}) - \text{ZPE}(\text{B}) - \delta^{\text{BSSE}} \quad (1)$$

where  $\Delta E_{\text{el}} = E_{\text{AB}}^{\text{AB}} - E_{\text{A}}^{\text{A}} - E_{\text{B}}^{\text{B}}$ . Here  $E_{\text{Y}}^{\text{Z}}(\text{X})$  represents the energy of subsystem X at optimized geometry Y using the basis set Z and the counterpoise correction is defined as<sup>47</sup>

$$\delta^{\text{BSSE}} = E_{\text{AB}}^{\text{A}}(\text{A}) + E_{\text{AB}}^{\text{B}}(\text{B}) - E_{\text{AB}}^{\text{AB}}(\text{A}) - E_{\text{AB}}^{\text{AB}}(\text{B}) \quad (2)$$

For all the organic cyclic systems, we have computed one of the most effective structure-based indices of aromaticity, the harmonic oscillator model of aromaticity (HOMA) index,<sup>48</sup> defined by Kruszewski and Krygowski as

$$\text{HOMA} = 1 - \frac{\alpha}{n} \sum_{i=1}^n (R_{\text{opt}} - R_i) \quad (3)$$

where  $n$  is the number of bonds considered and  $\alpha$  is an empirical constant fixed to give HOMA = 0 for a model nonaromatic system and HOMA = 1 for a system with all bonds equal to an optimal value  $R_{\text{opt}}$ , assumed to be achieved for fully aromatic systems.  $R_i$  stands for a running bond length.

As electronic indices of aromaticity,<sup>49</sup> we have used the para-delocalization (PDI) and aromatic fluctuation (FLU) indices. Both indices require the calculation of the delocalization index (DI)<sup>50</sup> that is obtained from the double integration of the exchange-correlation density over the atomic basins defined

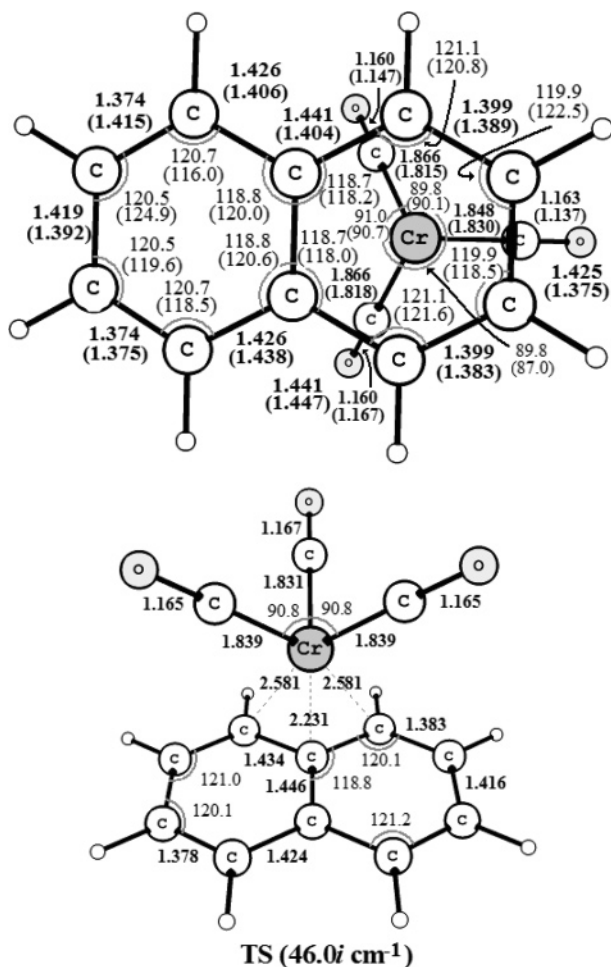


**Figure 1.** Optimized reactant and transition state structures involved in the haptotropic rearrangement on the naphthalene molecule. Experimental values<sup>59</sup> are in parenthesis. Distances in Å and angles in degrees.

within the theory of Atoms in Molecules.<sup>51</sup> The expression for the DIs reads as

$$\delta(A,B) = -2 \int_B \int_A \Gamma_{XC}(\vec{r}_1, \vec{r}_2) d\vec{r}_1 d\vec{r}_2 \quad (4)$$

This term is a quantitative measure of the number of electron pairs delocalized or shared between atomic basins A and B. The PDI<sup>52</sup> took the average para-DI in 6-MRs as a measure of local aromaticity, in which there are three para-related positions, namely (1,4), (2,5), and (3,6)

$$PDI = \frac{\delta(1,4) + \delta(2,5) + \delta(3,6)}{3} \quad (5)$$

The formula below was given for FLU<sup>53</sup>

$$FLU = \frac{1}{n} \sum_{A-B}^{RING} \left[ \left( \frac{V(B)}{V(A)} \right)^\alpha \left( \frac{\delta(A,B) - \delta_{ref}(A,B)}{\delta_{ref}(A,B)} \right)^2 \right] \quad (6)$$

where the summation runs over all adjacent pairs of atoms around the ring,  $n$  is equal to the number of atoms of the ring,  $V(A)$  is the global delocalization of atom A defined as  $V(A) = \sum_{A \neq B} \delta(A,B)$  and

$$\alpha = \begin{cases} 1 & V(B) > V(A) \\ -1 & V(B) \leq V(A) \end{cases} \quad (7)$$

$\delta(A,B)$  and  $\delta_{ref}(A,B)$  are the DI values for the atomic pairs A and B and its reference value, respectively. The second factor in eq 6 measures the relative divergence with respect to a typical aromatic system and the first factor penalizes those with highly localized electrons. The reference DI value for the C–C bond ( $\delta_{ref}(C,C) = 1.4$  e) was obtained from benzene at the HF/6-31G(d) level of theory. All indices of aromaticity have been obtained at the B3LYP/(Watchers' basis,6-31G(d,p)) level of theory.

Through the ADF package developed by Baerends et al.,<sup>54</sup> we carried out molecular orbital (MO) and bond energy decomposition analyses (EDA) between the PAH and the  $Cr(CO)_3$  fragments. In the EDA, the total bond energy  $\Delta E$  is composed of two principal components

$$\Delta E = \Delta E_{prep} + \Delta E_{int} \quad (8)$$

These terms are defined as follows: the preparation energy  $\Delta E_{prep}$  is the amount of energy required to deform the separate molecular fragments from their equilibrium structure to the geometry they acquire in the final complex; the interaction energy  $\Delta E_{int}$  corresponds to the actual energy change when the prepared fragments are combined to form the complex, which at the same time can be decomposed using a Morokuma-type scheme into<sup>55</sup>

$$\Delta E_{int} = \Delta V_{elstat} + \Delta E_{Pauli} + \Delta E_{oi} \quad (9)$$

The term  $\Delta V_{elstat}$  corresponds to the classical electrostatic interaction between the unperturbed charge distributions of the deformed fragments and is usually attractive. The Pauli repulsion  $\Delta E_{Pauli}$  comprises the destabilizing interactions between occupied orbitals. It arises as the energy change associated when going from the superposition of the unperturbed electron densities of the two fragments, PAH and  $Cr(CO)_3$ , to the final wave function (which is normalized and antisymmetrized at this point, obeying the Pauli principle) and this difference comprises the four-electron destabilizing interactions between occupied orbitals and is responsible for any steric repulsion. The orbital interaction,  $\Delta E_{oi}$ , accounts for electron-pair bonding, charge transfer (e.g., donation and backdonation between these two fragments), and polarization (empty-occupied orbital mixing on one fragment due to the presence of another fragment). For the EDA study using ADF, we have employed the BLYP functional<sup>42,56</sup> together with an uncontracted all-electron triple- $\zeta$  basis set augmented by two extra polarization functions for Cr, C, H and O atoms.<sup>57</sup>

All of the figures of the molecular geometries were generated by using the ChemCraft visualization program.<sup>58</sup>

### 3. Results and Discussion

This section is organized as follows. First, we present the molecular structures and relative energies of the most stable conformer of reactants, intermediates, and TSs present in the four rearrangements studied. Second, we perform MO and EDA analyses to get a deeper insight into the effect of the PAH size and its curvature. And finally, we briefly analyze the changes in aromaticity in PAHs after the  $Cr(CO)_3$  coordination.

**3.1. Reaction Mechanisms of Haptotropic Migration.** Let us begin with the simplest tricarbonylchromium IRHR occurring in the  $(\eta^6-C_{10}H_8)Cr(CO)_3$  complex. The optimized geometry of the most stable conformer found on the PES is shown in Figure 1. From the Cr–C distances, it is found that this is a nontotally symmetric  $\eta^6$ -coordinated molecule, with the position of the  $Cr(CO)_3$  tripod slightly shifted (0.18 Å) from the ring center



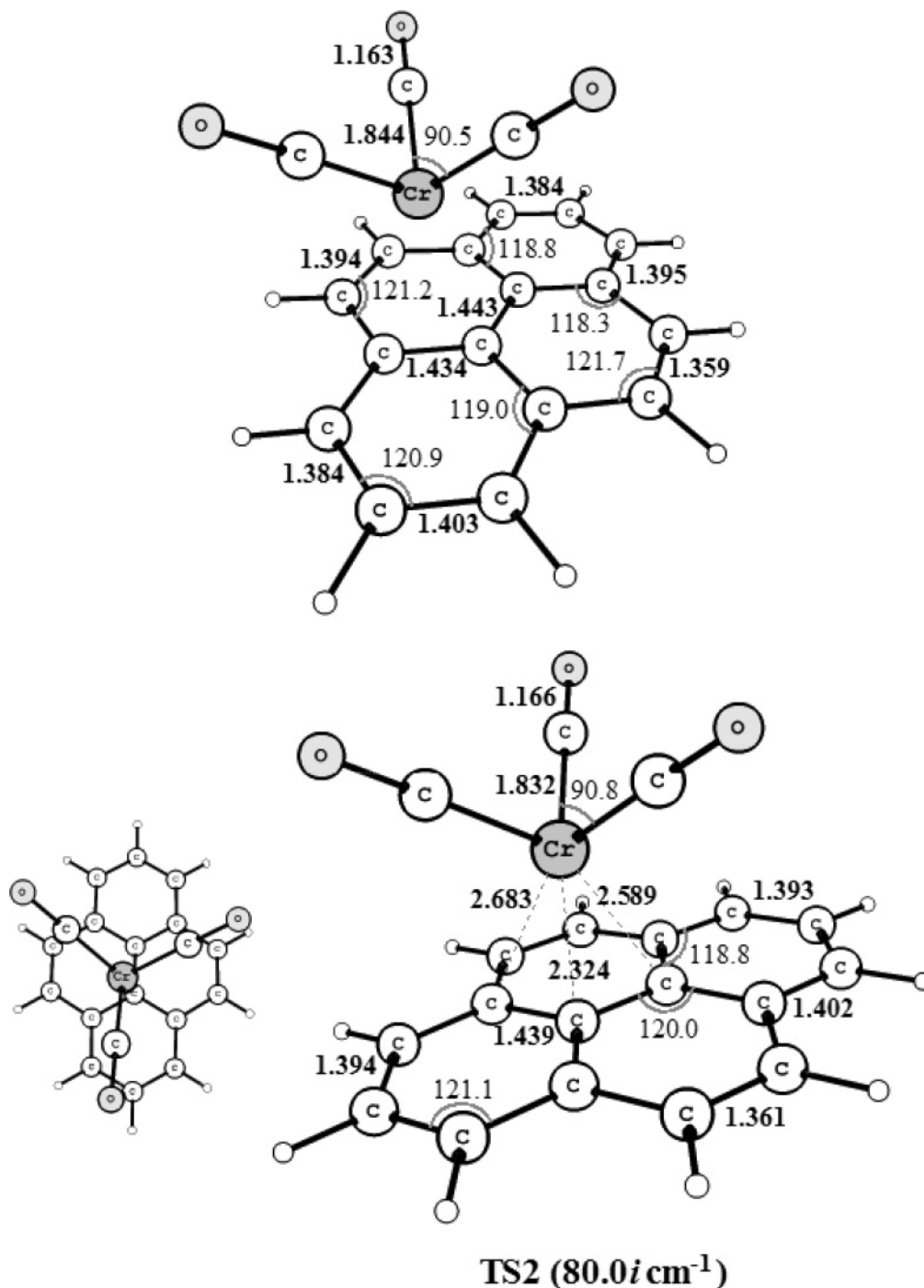


**Figure 2.** Optimized reactant and transition state found for the tricarbonylchromium migration on the pyrene fragment. Distances in Å and angles in degrees.

toward the most external C–C bond (parallel to the bond between the two rings).<sup>27</sup> As can be seen in Figure 1, the calculated geometry is in good agreement with the X-ray structural measurements of  $(\eta^6\text{-C}_{10}\text{H}_8)\text{Cr}(\text{CO})_3$ .<sup>59</sup> The metal tripod is placed staggered with respect to the naphthalene ( $D_{2h}$ ,  $^1A_g$ ) C–H bonds to reduce steric repulsions. The distance of chromium to the ring center is about 1.79 Å, a slightly longer distance compared to benzene–Cr interaction of 1.720 Å (exp.: 1.724–1.726 Å)<sup>60</sup> at the B3LYP/6-31G(d,p) level of theory,<sup>39</sup> reflecting the effect of increasing the size of the system in the metal complexation as we will discuss further later. The calculated binding energy of the naphthalene–Cr bond is 50.2 kcal·mol<sup>-1</sup> not too far from the experimental value<sup>27</sup> of  $6 \pm 2$  kcal·mol<sup>-1</sup> less than the benzene–Cr bond in the  $(\eta^6\text{-C}_6\text{H}_6)\text{Cr}$ –

(CO)<sub>3</sub> complex for which the binding energy is  $43 \pm 3$  kcal·mol<sup>-1</sup> according to Brown et al.<sup>61</sup> and 53 kcal·mol<sup>-1</sup> as found by Mukerjee and co-workers,<sup>24</sup> respectively, and in line with previous reported data.<sup>4,27</sup> The rotation of the tripod by 60° about its local approximate  $C_3$  axis generates another stable conformer higher in energy that will not be analyzed in the present work. Let us briefly add here that in this kind of complexes the extremely low rotational barriers makes the rotational movement of the Cr(CO)<sub>3</sub> tripod basically free.<sup>43,62</sup>

In the search of the haptoisomerization reaction pathway, we located on the PES a TS (see Figure 1) in which the chromium is attached to a single carbon atom in an  $\eta^1$ -fashion. Our intrinsic reaction coordinate (IRC) calculations starting from the obtained TS fail to locate the energy minimum of  $\eta^3$ -allyl type postulated

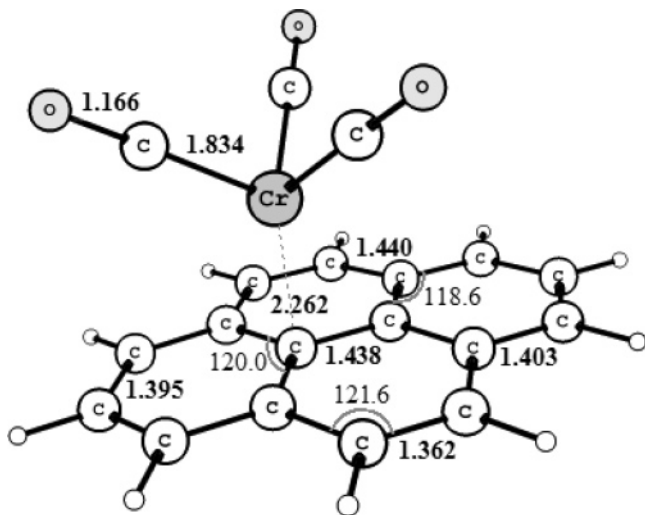


**Figure 3.** Intermediate ( $\eta^1$ -pyrene)tricarbonylchromium that connects the two equivalent transition states along the reaction pathway of the haptotropic isomerization. Distances in Å and angles in degrees.

by Albright, Hoffmann, and co-workers.<sup>4</sup> A similar result was reported by the groups of Oprunenko<sup>10</sup> and Dolg.<sup>29</sup> As the migration proceeds from the reactant to the TS, the  $\text{Cr}(\text{CO})_3$  tripod rotates by ca. 30°. We also found the  $\eta^2$ -structure corresponding to the highest energy point in the least-motion pathway of the IRHR where the chromium passes through the middle of the C–C bond between the two rings. This structure is a three-order saddle-point (one frequency moving to the two equivalent forms of the found  $\eta^1$ -TS, a second is the rotation of the tripod and the third is the desired haptotropic migration), thus reinforcing the previous results obtained using lower levels of theory.<sup>4,6,27</sup> Such a hypothetical three-order  $\eta^2$ -TS is 11.8 kcal·mol<sup>-1</sup> higher in energy than the  $\eta^1$ -TS shown in Figure 1. This fact remains true for every other reaction mechanism in our study. The reason for the  $\text{Cr}(\text{CO})_3$  tripod rotation and for the higher energy of the least-motion path as compared to the pathway along the  $\eta^1$ -TS was discussed in detail through an orbital interaction diagram by Albright, Hoffmann and co-workers.<sup>4</sup> The calculated activation barrier for the migration of  $\text{Cr}(\text{CO})_3$  over naphthalene is 25.7 kcal·mol<sup>-1</sup> (experimental kinetic parameters goes from 21.1–26.6 kcal·mol<sup>-1</sup> for naphthalene substituted derivatives in the haptotropic change<sup>2,23</sup>). This value is close to previous reported theoretical DFT energy barriers for this process of about 30 kcal·mol<sup>-1</sup>.<sup>10,16,29</sup>

For the case of the ( $\eta^6$ - $\text{C}_{16}\text{H}_{10}$ ) $\text{Cr}(\text{CO})_3$  complex, the geometrical parameters of the optimized reactants, intermediate, and TS are shown in Figures 2 and 3. As pointed out above, experimentally the  $\text{Cr}(\text{CO})_3$  fragment in this complex is attached to the less substituted and outer ring.<sup>8</sup> However, since we want to analyze the IRHR in an analogous environment, we have analyzed the IRHR between the less stable isomers in which the  $\text{Cr}(\text{CO})_3$  fragment is coordinated to one of the inner rings of pyrene. It is worth noting that for the experimentally known ( $\eta^6$ - $\text{C}_{16}\text{H}_{10}$ ) $\text{Cr}(\text{CO})_3$  complex, structural experimental data on this complex<sup>8</sup> are in good agreement with our theoretical calculations (results not shown here). The structure of the studied reactant is depicted in Figure 2. As can be seen, the C–C distances of the Cr-coordinated ring are somewhat elongated in comparison with the distances of the neighboring rings. The chromium-ring center distance of 1.85 Å is a sign of lesser interaction of the  $\text{Cr}(\text{CO})_3$  fragment with the  $\pi$ -system of the organic part. Indeed, the binding energy (40.6 kcal·mol<sup>-1</sup>) for this position of the metal fragment on the pyrene molecule

( $\text{C}_{16}\text{H}_{10}$ ,  $D_{2h}$   $^1A_g$ ) is found to be about 10 kcal·mol<sup>-1</sup> lower than that of the ( $\eta^6$ -naphthalene) $\text{Cr}(\text{CO})_3$  complex.

We found the TS for ( $\eta^6$ - $\text{C}_{16}\text{H}_{10}$ ) $\text{Cr}(\text{CO})_3$  IRHR in a slightly  $\eta^3$ -position with respect to the central C–C bond of this PAH, as can be seen in Figure 2. The corresponding activation barrier is 19.8 kcal·mol<sup>-1</sup> and following the IRC forward we found an intermediate in which the chromium is bound in an  $\eta^1$ -mode to pyrene (see Figure 3). Similarly to what occurred in naphthalene, the  $\text{Cr}(\text{CO})_3$  tripod rotates ca. 20° as the migration proceeds from the reactant to the intermediate.

We now turn on to the haptomigration on dibenzo-[fg,op]-anthanthrene ( $\text{C}_{28}\text{H}_{14}$ ,  $D_{2h}$   $^1A_g$ ), which we have considered because is the formed structure next in size that keeps the symmetry of the naphthalenic rings by adding four 6-MRs at the corners of pyrene as can be seen in Scheme 1. The optimized molecular geometry of the ( $\eta^6$ - $\text{C}_{28}\text{H}_{14}$ ) $\text{Cr}(\text{CO})_3$  complex is depicted in Figure 4. As for pyrene, the isomer in Figure 4 is not necessarily the most stable ( $\eta^6$ - $\text{C}_{28}\text{H}_{14}$ ) $\text{Cr}(\text{CO})_3$  complex, but it is the one we have studied to discuss size effects in IRHRs. As compared to the ( $\eta^6$ - $\text{C}_{10}\text{H}_8$ ) $\text{Cr}(\text{CO})_3$  complex, the  $\text{Cr}(\text{CO})_3$  tripod is rotated by about 30° in the most stable conformer of the ( $\eta^6$ - $\text{C}_{28}\text{H}_{14}$ ) $\text{Cr}(\text{CO})_3$  isomer depicted in Figure 4. As said in the introduction this rotation is almost free,<sup>43,62</sup> so it is not surprising that it may change from one complex to the other. Interestingly, the chromium-ring center distance is now 1.94 Å, indicating that the interaction between the  $\text{C}_{28}\text{H}_{14}$  and the  $\text{Cr}(\text{CO})_3$  fragment in the ( $\eta^6$ - $\text{C}_{28}\text{H}_{14}$ ) $\text{Cr}(\text{CO})_3$  complex is weaker than that found in the ( $\eta^6$ - $\text{C}_{16}\text{H}_{10}$ ) $\text{Cr}(\text{CO})_3$  complex. Indeed, the calculated binding energy for this complex is 22.9 kcal·mol<sup>-1</sup>. For this case, we also found two TSs in an  $\eta^3$ -position with respect to the central carbons as for the pyrene system. Both of them connect the reactant or the product and the intermediate structure shown in Figure 5. In this intermediate, the chromium atom is bound to one of the central carbon atoms (Cr–C distance of 2.19 Å, see Figure 5), thus leading to an analogous reaction pathway for the IRHR as that one found for pyrene. The activation barrier for the IRHR in this system is as low as 6.2 kcal·mol<sup>-1</sup>.

Finally, we considered the cyclopenta-[bc]-coronene ( $\text{C}_{26}\text{H}_{12}$ ,  $\text{C}_{2v}$   $^1A_1$ ), a curved PAH which we have selected again preserving the symmetry of the haptomigration between the two central rings but for a nonplanar structure. The optimized geometry of  $\text{C}_{26}\text{H}_{12}$  attached to the tricarbonylchromium complex is shown in Figure 6. Distances of C–C bonds for the coordinated ring do not differ significantly from those in the non-coordinated rings. The Cr–ring center distance of 1.89 Å indicates that the interaction is stronger than that of  $\text{C}_{28}\text{H}_{14}$ , a planar PAH of similar size. Indeed, the calculated binding energy for this complex is 30.2 kcal·mol<sup>-1</sup>, i.e., 7.3 kcal·mol<sup>-1</sup> larger than that of  $\text{C}_{28}\text{H}_{14}$ . This fact is in agreement with a previous calculation of Nunzi et al.<sup>28</sup> who found that the binding energy to a nanotube sidewall is about 10.3 kcal·mol<sup>-1</sup> higher than in circumcoronene. Having a curved surface,  $\text{C}_{26}\text{H}_{12}$  could be coordinated both in the concave (endo) or the convex (exo) side. We have checked that the  $\text{Cr}(\text{CO})_3$  complex coordinates only in the convex side. Some experimental and theoretical studies in literature related to the  $\text{Cr}(\text{CO})_3$  coordination on corannulene and other curved PAHs found in most cases that the exo haptomer is more stable than endo coordination.<sup>20,31–33,63</sup> In the case of our system, the  $\text{Cr}(\text{CO})_3$  coordination to the concave side induces a bowl-to-bowl inversion during the optimization geometry process that leads to the exo coordinated ( $\eta^6$ - $\text{C}_{26}\text{H}_{12}$ ) $\text{Cr}(\text{CO})_3$  complex. This bowl-to-bowl inversion is favored by the flattening occurring in the  $\text{C}_{26}\text{H}_{12}$  surface after  $\text{Cr}(\text{CO})_3$  coordination (the average

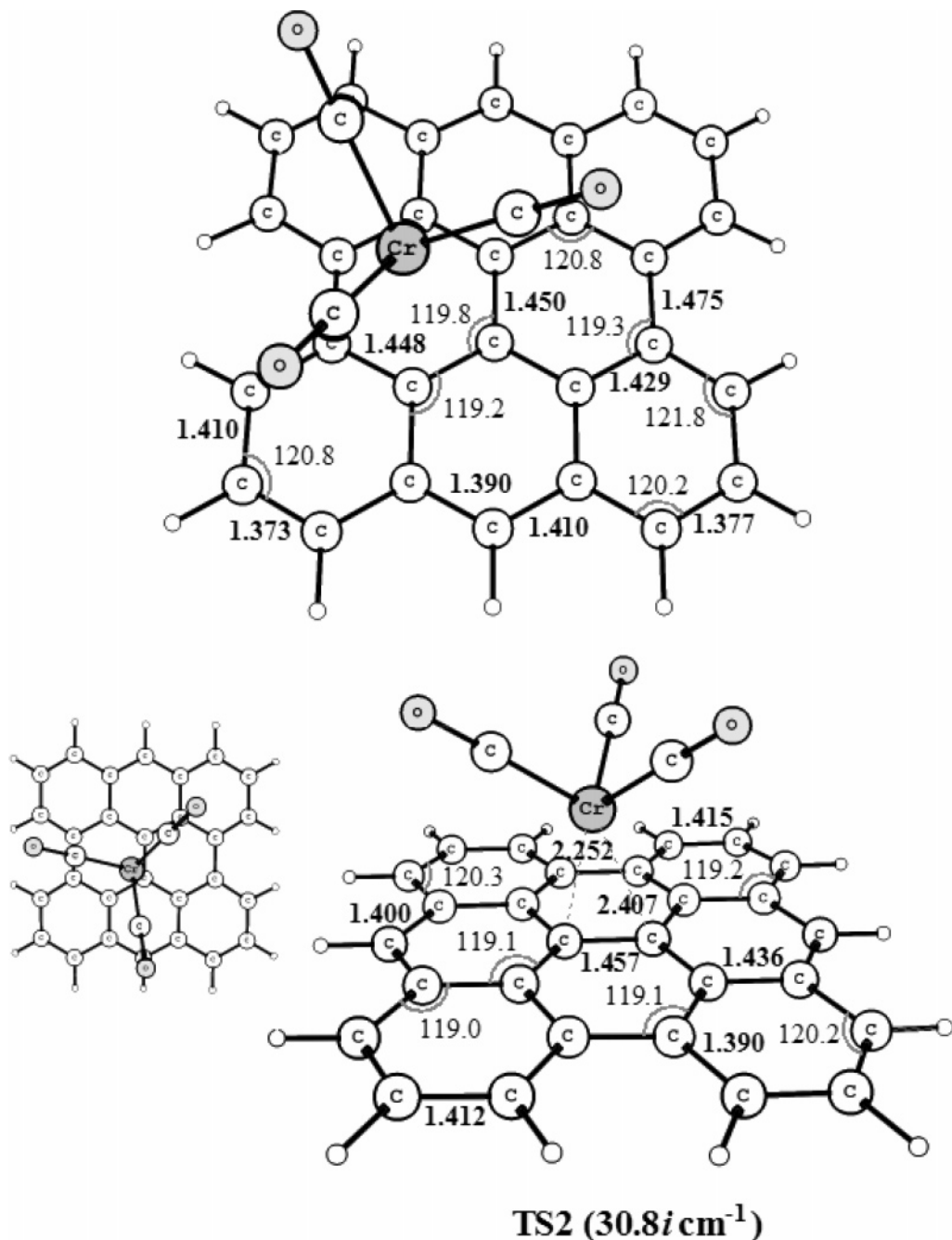


**Figure 4.** Optimized geometrical structures of the reactant and the transition state involved in the haptotropic rearrangement studied on the dibenzo-[fg,op]-anthanthrene species. Distances in Å and angles in degrees.

pyramidalization angle<sup>64</sup> of carbon atoms in C<sub>26</sub>H<sub>12</sub> changes from 3.1° in free C<sub>26</sub>H<sub>12</sub> to 2.8° in coordinated ( $\eta^6$ -C<sub>26</sub>H<sub>12</sub>)Cr(CO)<sub>3</sub>.<sup>32</sup>

For the IRHR in the ( $\eta^6$ -C<sub>26</sub>H<sub>12</sub>)Cr(CO)<sub>3</sub> complex, we found a unique TS in an  $\eta^1$ -coordination mode connecting reactants and products (see Figure 6). The activation barrier for the IRHR is just 13.3 kcal·mol<sup>-1</sup>, about half of the energy barrier calculated for the naphthalene substrate. Nunzi et al. investigated the haptotropic rearrangement of the Cr(CO)<sub>3</sub> on a carbon nanotube sidewall and they obtained a similar energy barrier of 16.2 kcal·mol<sup>-1</sup> for that curved system.<sup>28</sup>

As a summary of this section, bonding energies, activation barriers, and relative energies for the intermediates found for the analyzed IRHRs are listed in Table 1. It is important to emphasize that we observe an important reduction in both binding energy and energy barrier in the order naphthalene >

pyrene > dibenzo-[fg,op]-anthanthrene, i.e., the interaction of the Cr(CO)<sub>3</sub> unit decreases as the size increases and this facilitates IRHRs. On the other hand, the comparison between curved C<sub>26</sub>H<sub>12</sub> and planar C<sub>28</sub>H<sub>14</sub> of similar size leads to the conclusion that the curvature of the PAHs favors the coordination of the Cr(CO)<sub>3</sub> complex and makes the IRHRs more difficult.

As discussed in the case of the naphthalene species, there is a ring slippage that makes the  $\eta^6$ -coordination of the PAH to the metal fragment nontotally symmetric. This effect in the ( $\eta^6$ -C<sub>10</sub>H<sub>8</sub>)Cr(CO)<sub>3</sub> species has been discussed before by some authors<sup>4,65</sup> and has been also reported in other complexes.<sup>27,66</sup> The slippage in ( $\eta^6$ -C<sub>10</sub>H<sub>8</sub>)Cr(CO)<sub>3</sub> can be justified by the presence of a node at the central bonding in the HOMO and HOMO-3 orbitals of naphthalene (vide supra). The value of the slippage found in our four studied systems is given in Figure

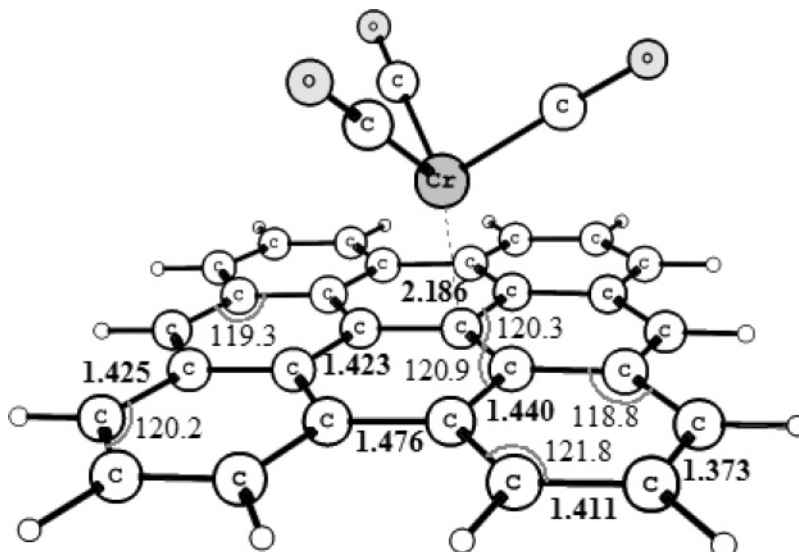


**Figure 5.** Intermediate ( $\eta^1$ -C<sub>26</sub>H<sub>14</sub>)tricarbonylchromium connecting the two equivalent transition states along the reaction pathway of the haptotropic isomerization studied. Distances in Å and angles in degrees.

**TABLE 1: Binding Energies ( $\Delta E$ ), Activation Barriers ( $\Delta E^\ddagger$ ), and Relative Energy of the Intermediate 2 ( $\Delta E_2$ ) with Respect to the ( $\eta^6$ -PAH)Cr(CO)<sub>3</sub> Reactant for the Two Reaction Routes Found at Level B3LYP/(Wachters' Basis, 6-31G(d,p))<sup>a</sup>**

route A	$\Delta E$	$\Delta E_2$	$\Delta E^\ddagger_{(1-TS2)}$
C <sub>16</sub> H <sub>10</sub>	-38.23	18.96	19.80
C <sub>28</sub> H <sub>14</sub>	-22.93	5.66	6.21
route B	$\Delta E$	$\Delta E_2$	$\Delta E^\ddagger_{(1-TS1)}$
C <sub>10</sub> H <sub>8</sub>	-50.16	-	25.71
C <sub>26</sub> H <sub>12</sub>	-30.23	-	13.26

<sup>a</sup> For the notation of the calculated structures see Figure 8. All energies (in kcal·mol<sup>-1</sup>) are corrected by BSSE.

7. We can see that ring slippage vanishes when the system becomes bigger for this series of PAHs irrespective of their curvature. As the size of the system grows and more  $\pi$  orbitals are involved in the bonding, the relevance of the orbitals with a central node becomes smaller. Finally, it is also worth noting that we have found two kinds of reaction pathways (A and B) for the IRHRs in the four PAHs studied which are sketched in Figure 8. In the next section, we will provide a reason to explain why a given PAH presents a reaction pathway A or B.

**3.2. Molecular Orbital and Energy Decomposition Analyses.** As we have seen in the previous section, the size of the PAH reduces the binding energy and favors the IRHR while the effect of the curvature is just the opposite. To obtain a better understanding of the reasons for this behavior, we have performed MO and EDA analyses with the help of the ADF program (see Computational Details).

In 1983, Hoffmann and co-workers<sup>4</sup> discussed the bonding mechanism in the ( $\eta^6$ -C<sub>10</sub>H<sub>8</sub>)Cr(CO)<sub>3</sub> complex through an orbital interaction diagram using the extended Hückel method. Their landmark analysis found that the dominant bonding interactions are those occurring between the two lowest unoccupied molecular orbitals (LUMOs) of Cr(CO)<sub>3</sub> and the three highest occupied molecular orbitals (HOMOs) of naphthalene with also some other minor contributions. This is indeed what can be seen in our MO interaction diagram of Figure 9. On the left and right sides, the highest-lying filled  $\pi$  orbitals of naphthalene and pyrene are displayed, whereas in the center of Figure 9, the LUMOs ( $a_1$  and  $e$ ) of the Cr(CO)<sub>3</sub> fragment are shown. We have adopted the notation used by Hoffmann and co-workers<sup>4</sup>

of  $s$  and  $a$  subscripts according to whether the orbital is symmetric or antisymmetric respect to the plane of  $C_s$  symmetry ( $yz$ ) of the initial ( $\eta^6$ -C<sub>10</sub>H<sub>8</sub>)Cr(CO)<sub>3</sub> complex (Figure 1). The numbers in Figure 9 represent the composition of the MOs of the ( $\eta^6$ -PAH)Cr(CO)<sub>3</sub> complex in terms of Gross Mulliken contributions.<sup>67</sup> The first evident characteristic observed when the polycyclic system grows up from naphthalene to pyrene is the reduction of the gap between the HOMO of the PAH and the LUMO of Cr(CO)<sub>3</sub>. We would expect that this brings in consequence an increase in orbital interactions as HOMOs from the organic part get close in energy to LUMOs of the metal fragment. However, these interactions become weaker (MOs formed are less stabilized in the pyrene system) and the contributions from the LUMOs of the Cr(CO)<sub>3</sub> fragment to the MOs of the complex are smaller. This fact can be explained by the observed decrease in the overlap between the HOMOs of the PAH and the LUMOs of Cr(CO)<sub>3</sub> when going from naphthalene to pyrene: HOMO ( $\pi_a/\pi_s$ ) - LUMO+1 ( $e_a$ /LUMO ( $e_s$ ), 0.12 to 0.07; HOMO-1/HOMO-2 ( $\pi_s$ ) - LUMO ( $e_s$ ), 0.09 to 0.02; HOMO-2/HOMO-1 ( $\pi_a$ ) - LUMO ( $e_a$ ), 0.22 to 0.14. Thus, when the size of the PAH increases, the number of atoms contributing to each MO of the PAH grows up and, consequently, the coefficients of each atomic orbital become smaller. This translates into a reduction of the overlap between the HOMOs of the PAH and the LUMOs of Cr(CO)<sub>3</sub> thus explaining why the ( $\eta^6$ -PAH)-Cr(CO)<sub>3</sub> bonding is reduced when the organic fragment becomes bigger.

The effect of the curvature can be discussed by comparing the MOs of the planar C<sub>28</sub>H<sub>14</sub> and the curved C<sub>26</sub>H<sub>12</sub> species (see the Supporting Information, Figure S1). There are two factors that explain the higher binding energy in ( $\eta^6$ -C<sub>26</sub>H<sub>12</sub>)-Cr(CO)<sub>3</sub> as compared to ( $\eta^6$ -C<sub>28</sub>H<sub>14</sub>)-Cr(CO)<sub>3</sub>. First, the HOMOs of the curved PAH that intervene more in the bonding mechanism are higher in energy than those of the planar species with the only exception of the HOMO of C<sub>28</sub>H<sub>14</sub>. Second, the HOMOs present larger lobes in the convex surface leading to better MO overlaps: the overlaps of the LUMOs of Cr(CO)<sub>3</sub> with the HOMOs of the planar C<sub>28</sub>H<sub>14</sub> and the curved C<sub>26</sub>H<sub>12</sub> are in the range 0.02–0.05 and 0.10–0.16, respectively.

We have seen in the previous section that some IRHRs involve an intermediate structure and two TSs and others just a unique TS. Figure 10 contains a schematic orbital interaction between the HOMO-2 ( $\pi_s$ ) and LUMO ( $e_s$ ) in pyrene in



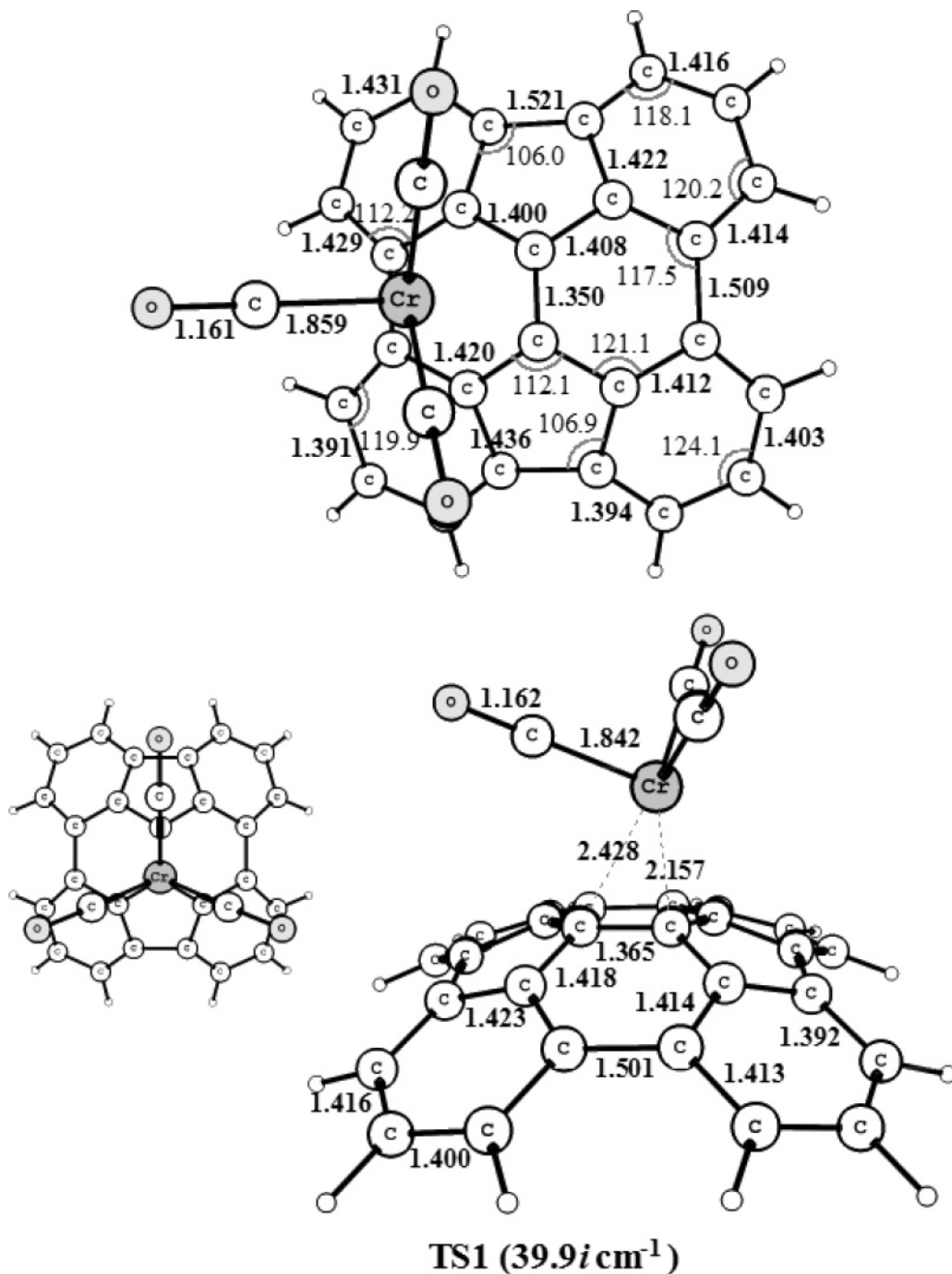


**Figure 6.** Optimized structures of the stationary points involved in the haptotropic change from one six-membered ring to another in the curved cyclopenta-[bc]-coronene derivative. Distances in Å and angles in degrees.

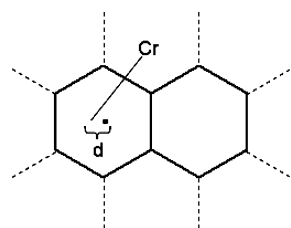


**Figure 7.** Ring slippage *d* reported for the four reactants ( $\eta^6$ -PAH)-Cr(CO)<sub>3</sub> analyzed.

Complex	<i>d</i> (Å)
Cr(CO) <sub>3</sub> + C <sub>10</sub> H <sub>8</sub>	0.18
Cr(CO) <sub>3</sub> + C <sub>16</sub> H <sub>10</sub>	0.11
Cr(CO) <sub>3</sub> + C <sub>26</sub> H <sub>12</sub>	0.07
Cr(CO) <sub>3</sub> + C <sub>28</sub> H <sub>14</sub>	0.02

reactants, intermediate, and TS. As can be seen in the picture as compared with the TS in the intermediate structure there is an extra overlap coming from the C atom located in one of the outer pyrene rings that are not affected by the studied IRHR that explains the formation of this intermediate in pyrene. The

same occurs also in C<sub>28</sub>H<sub>14</sub>, while such extra stabilization exist neither in naphthalene nor in curved C<sub>26</sub>H<sub>12</sub>, justifying the lack of intermediate in these systems.

To get a deeper insight into the bonding mechanism in ( $\eta^6$ -PAH)-Cr(CO)<sub>3</sub> complexes and the changes occurring along the reaction paths, we have performed an EDA analysis of the binding energy between the PAH fragment and the Cr(CO)<sub>3</sub> moiety for reactants, intermediates, and TSs. EDA results in Tables 2 and 3 have been computed using the ADF program with the BLYP functional at the B3LYP optimized geometries discussed in the previous section. Therefore, total bonding energies in Tables 2 and 3 are slightly different to those obtained at the B3LYP level (Table 1). However, the qualitative conclusion reached from our EDA analysis should not be altered significantly by the change in the functional.



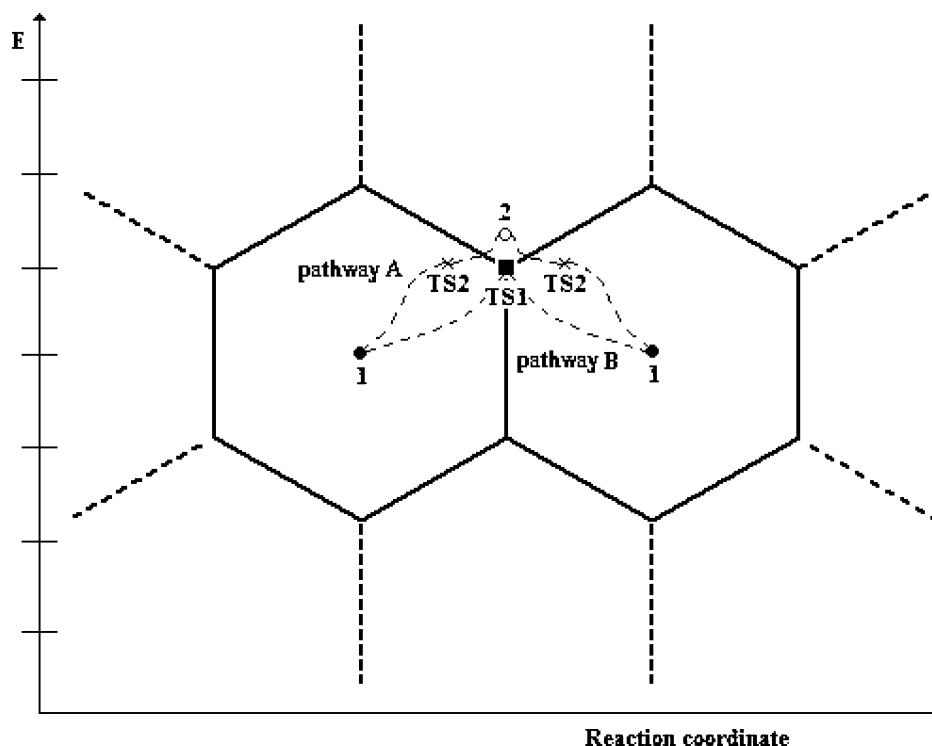


**Figure 8.** The two reaction pathways found for haptotropic migration (1). Pathway **A** involves an  $\eta^1$ -intermediate (2) whereas pathway **B** follows just one transition state.

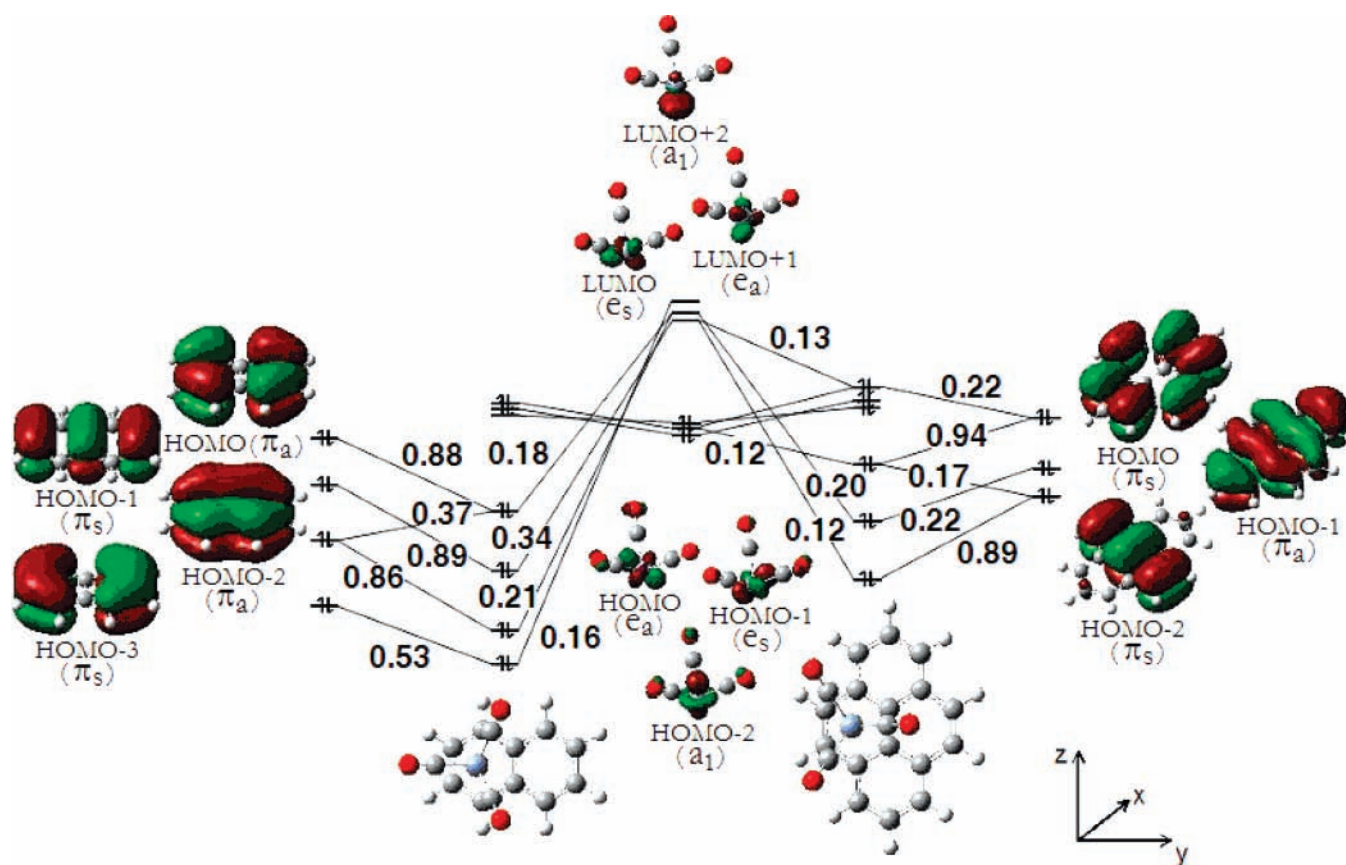


**Figure 9.** Orbital interaction diagram showing the comparison of naphthalene and pyrene systems interacting with the  $\text{Cr}(\text{CO})_3$  unit. The numbers represent the composition of the MOs in terms of Gross Mulliken contributions.

As can be seen in Tables 2 and 3, the  $\Delta E_{\text{prep}}$  term is quite small for all species analyzed. It decreases as the number of rings increases indicating that bigger PAHs need less energy to become distorted. The dominant term for these complexes is the steric repulsion,  $\Delta E_{\text{Pauli}}$ , but the other contributions (orbital

interaction and electrostatic terms) overpass it to sustain joined these molecules. An interesting observation is that the orbital interaction component represent 54.8 – 62.1% of the total stabilizing interactions ( $\Delta E_{\text{oi}} + \Delta V_{\text{elstat}}$ ) while the electrostatic term constitutes the 37.9–45.2% depending on the PAH. Thus,

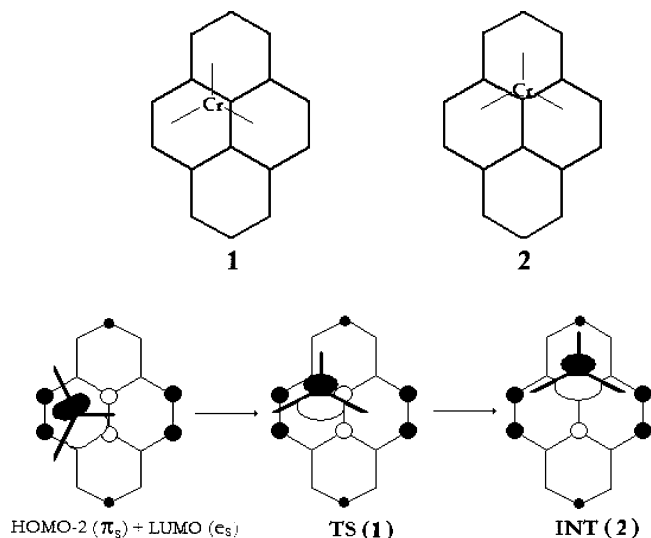


**Figure 10.** Interactions with the upper ring in pyrene stabilize intermediate 2.

**TABLE 2: EDA of the Binding Energy of Tricarbonylchromium to Naphthalene (Top) and Pyrene (Bottom) in the Haptotropic Isomerization at BLYP/TZ2P//B3LYP/(Wachters' Basis, 6-31G(d,p)) Level of Theory**

	C <sub>10</sub> H <sub>8</sub> CrCO <sub>3</sub>	TS (C <sub>10</sub> H <sub>8</sub> CrCO <sub>3</sub> )
$\Delta E_{oi}$	-107.42	-40.47
$\Delta E_{Pauli}$	138.84	53.86
$\Delta V_{elstat}$	-76.21	-33.34
$\Delta E_{int}$	-44.78	-19.95
$\Delta E_{prep}$	2.29	0.23
$\Delta E$	-42.49	-19.72

	C <sub>16</sub> H <sub>10</sub> CrCO <sub>3</sub>	TS (C <sub>16</sub> H <sub>10</sub> CrCO <sub>3</sub> )	I (C <sub>16</sub> H <sub>10</sub> CrCO <sub>3</sub> )
$\Delta E_{oi}$	-93.23	-35.77	-37.95
$\Delta E_{Pauli}$	119.48	44.26	48.89
$\Delta V_{elstat}$	-63.30	-24.47	-27.47
$\Delta E_{int}$	-36.04	-15.98	-16.53
$\Delta E_{prep}$	1.81	0.04	0.23
$\Delta E$	-34.23	-15.94	-16.30

**TABLE 3: EDA of the Binding Energy of Tricarbonylchromium to Cyclopenta-[bc]-coronene (Top) and Dibenzo-[fg,op]-anthanthrene (Bottom) in the Haptotropic Isomerization at BLYP/TZ2P//B3LYP/(Wachters' Basis, 6-31G(d,p)) Level of Theory**

	C <sub>26</sub> H <sub>12</sub> CrCO <sub>3</sub>	TS (C <sub>26</sub> H <sub>12</sub> CrCO <sub>3</sub> )
$\Delta E_{oi}$	-84.43	-52.39
$\Delta E_{Pauli}$	102.70	71.32
$\Delta V_{elstat}$	-51.72	-41.94
$\Delta E_{int}$	-33.45	-23.00
$\Delta E_{prep}$	1.58	1.11
$\Delta E$	-31.87	-21.89

	C <sub>28</sub> H <sub>14</sub> CrCO <sub>3</sub>	TS (C <sub>28</sub> H <sub>14</sub> CrCO <sub>3</sub> )	I (C <sub>28</sub> H <sub>14</sub> CrCO <sub>3</sub> )
$\Delta E_{oi}$	-72.75	-51.04	-51.66
$\Delta E_{Pauli}$	90.75	65.77	63.83
$\Delta V_{elstat}$	-44.44	-35.42	-33.34
$\Delta E_{int}$	-26.44	-20.68	-21.16
$\Delta E_{prep}$	0.96	0.55	0.55
$\Delta E$	-25.48	-20.13	-20.61

unsurprisingly, we find that the covalent contribution to the bond is more important than the electrostatic one. By comparing the absolute values of each binding energy given in Tables 2 and 3, we see that, not unexpectedly, the larger binding energy of the smaller or more curved PAHs goes with larger orbital interaction energies due to better overlaps (vide supra), and larger electrostatic and Pauli repulsions as a consequence of

**TABLE 4: Electron Donation (*D*) and Backdonation (*B*) and Charge on the CrCO<sub>3</sub> Fragment for the Reported Reaction Mechanisms (1 Stands for Reactant, TS for Transition State and 2 for Intermediate Structure) Calculated at BLYP/TZ2P//B3LYP/(Wachters' Basis, 6-31G(d,p)) Level of Theory**

	<i>D</i>	<i>B</i>	Hirshfeld	Voronoi
C <sub>10</sub> H <sub>8</sub> CrCO <sub>3</sub>				
1	0.69	0.92	-0.12	-0.12
TS1	0.21	0.37	-0.03	-0.03
C <sub>16</sub> H <sub>10</sub> CrCO <sub>3</sub>				
1	0.59	0.78	-0.11	-0.11
TS2	0.19	0.33	-0.02	-0.02
2	0.20	0.33	-0.01	-0.01
C <sub>26</sub> H <sub>12</sub> CrCO <sub>3</sub>				
1	0.61	0.70	-0.13	-0.14
TS1	0.43	0.37	-0.14	-0.14
C <sub>28</sub> H <sub>14</sub> CrCO <sub>3</sub>				
1	0.54	0.46	-0.11	-0.11
TS2	0.42	0.45	-0.09	-0.09
2	0.38	0.43	-0.06	-0.06

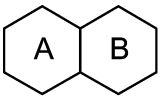
the fact that the Cr(CO)<sub>3</sub> is located closer to the PAHs. The same occurs when, for a given PAH, we compare the reactant with the TS or the intermediate. Orbital interactions are reduced in the TS and/or intermediate and this reduction is followed by a decrease of the electrostatic interactions and Pauli repulsions. An interesting conclusion can be observed comparing the C<sub>26</sub>H<sub>12</sub> and C<sub>28</sub>H<sub>14</sub> species: in a proportional comparison  $\Delta E_{Pauli}/\Delta E$ , the steric repulsion is less for the curved ( $\eta^6$ -C<sub>26</sub>H<sub>12</sub>)Cr(CO)<sub>3</sub> derivative than for ( $\eta^6$ -C<sub>28</sub>H<sub>14</sub>)Cr(CO)<sub>3</sub> species (Table 5).

Finally, the electron  $\pi$ -donation from the Cr(CO)<sub>3</sub> fragment to the PAH and the  $\sigma$ -backdonation from the PAH to the Cr(CO)<sub>3</sub> fragment as well as the total charges on the Cr(CO)<sub>3</sub> fragment are listed in Table 4. As expected from its electron withdrawing character, the total electronic charge on the Cr(CO)<sub>3</sub> fragment is negative. It is worth noting that in almost all cases  $\sigma$ -backdonation is dominant over  $\pi$ -donation, as expected from our previous MO analysis. One can also appreciate from the results of Table 4 that the donation and backdonation electronic exchange between the arene and the Cr(CO)<sub>3</sub> fragment is reduced as the number of rings increases, supporting our previous analysis. The same trend is found when one compares the curved ( $\eta^6$ -C<sub>26</sub>H<sub>12</sub>)Cr(CO)<sub>3</sub> and the planar ( $\eta^6$ -C<sub>28</sub>H<sub>14</sub>)Cr(CO)<sub>3</sub> species; that is, electronic exchange is larger for the curved species which has a larger binding energy.

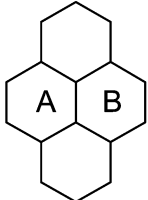
### 3.3. Aromaticity Changes Due to Cr(CO)<sub>3</sub> Coordination.

A final motivation for the present research has been to analyze the aromaticity changes in a PAH when it is interacting with a Cr(CO)<sub>3</sub> moiety. As explained in the Introduction section there is some controversy about whether there is a reduction or an increase in aromaticity of the ring after coordination with the Cr(CO)<sub>3</sub> complex. We have used here three local aromaticity indices referred in literature to test aromaticity in our studied molecules, namely, PDI, FLU, and HOMA. These indices use different criteria to define aromaticity as described in the Computational Details section. The NICS indicator of aromaticity has not been considered since in a recent work on ( $\eta^6$ -C<sub>6</sub>H<sub>6</sub>)Cr(CO)<sub>3</sub> species we showed that NICS fails to account for the aromaticity in these kind of systems.<sup>39</sup>

In Tables 5 and 6, we gather the values of these indices for the central rings (the common skeleton of these systems of our interest) of each optimized minimum. For all indices and for all systems analyzed, there is a reduction in aromaticity for both the coordinated- (ring **A**) and non-coordinated ring (ring **B**) when going from the free PAH to the coordinated ( $\eta^6$ -PAH)-Cr(CO)<sub>3</sub> species. In most cases, the reduction of aromaticity is larger in ring **A** than in **B**. Unexpectedly, however, for pyrene,

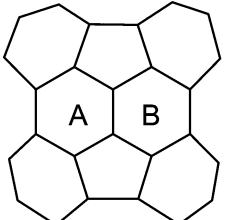
**TABLE 5: Aromaticity Indices of the Rings Where Haptotropic Migration Occurs for Naphthalene and Pyrene Species<sup>a</sup>**


INDEX	C <sub>10</sub> H <sub>8</sub>	C <sub>10</sub> H <sub>8</sub> Cr(CO) <sub>3</sub>	
		A	B
PDI	0.075	0.031	0.071
FLU	0.010	0.016	0.013
HOMA	0.769	0.592	0.719

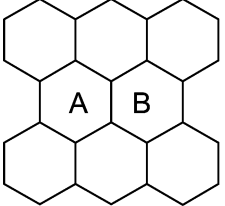


INDEX	C <sub>16</sub> H <sub>10</sub>	C <sub>16</sub> H <sub>10</sub> Cr(CO) <sub>3</sub>	
		A	B
PDI	0.043	0.025	0.034
FLU	0.020	0.023	0.027
HOMA	0.550	0.436	0.388

<sup>a</sup> **A** is the ring coordinated to Cr(CO)<sub>3</sub> complex and **B** is the non-coordinated ring. PDI are in electrons.

**TABLE 6: Aromaticity Indices of the Rings Where Haptotropic Migration Occurs for C<sub>26</sub>H<sub>12</sub> and C<sub>28</sub>H<sub>14</sub> Species<sup>a</sup>**


INDEX	C <sub>26</sub> H <sub>12</sub>	C <sub>26</sub> H <sub>12</sub> Cr(CO) <sub>3</sub>	
		A	B
PDI	0.037	0.024	0.028
FLU	0.018	0.028	0.027
HOMA	0.287	0.266	0.226



INDEX	C <sub>28</sub> H <sub>14</sub>	C <sub>28</sub> H <sub>14</sub> Cr(CO) <sub>3</sub>	
		A	B
PDI	0.024	0.018	0.022
FLU	0.024	0.031	0.028
HOMA	0.238	0.065	0.201

<sup>a</sup> **A** is the ring coordinated to Cr(CO)<sub>3</sub> complex and **B** is the non-coordinated ring. PDI are in electrons.

HOMA and FLU indicate a larger reduction in ring **B** than in **A**. For HOMA, the same is found in the ( $\eta^6$ -C<sub>26</sub>H<sub>12</sub>)Cr(CO)<sub>3</sub> species, although in general ring **B** is more aromatic than **A**, as one could expect from the fact that the coordinated ring is the one interacting more strongly with the Cr(CO)<sub>3</sub> moiety.

#### 4. Conclusions

We have studied four reaction mechanisms of IRHR to provide insight into these intriguing reactions. The minimal energy path of the haptotropic migration of the metal follows a change in the coordination mode  $\eta^6 \rightarrow \eta^1 (\eta^3) \rightarrow \eta^6$  for the studied cases. The size of the polycyclic system reduces the haptoisomerization barrier while the curvature of the organic fragment favors interactions with the transition metal slowing down the haptotropic change.

It is found that there are two kinds of reaction pathways (**A** and **B**) for the IRHRs analyzed in this work. We have suggested that the presence of an intermediate structure in route **A** becomes favored when there is an extra overlap between the LUMO ( $e_s$ ) of the Cr(CO)<sub>3</sub> moiety and the HOMO of the PAH with suitable symmetry coming from a carbon atom located in an outer ring

perpendicular to the haptoisomerization route. We also have rationalized these results in terms of an EDA analysis. Aromaticity indices, in line with our previous findings, show that the interaction PAH-Cr(CO)<sub>3</sub> decreases the aromaticity of the coordinated ring.

**Acknowledgment.** Financial help has been furnished by the Spanish Ministerio de Educación y Cultura (MEC) Project No. CTQ2005-08797-C02-01/BQU and by the Catalan Departament d'Universitats, Recerca i Societat de la Informació (DURSI) of the Generalitat de Catalunya Project No. 2005SGR-00238. J.O.C.J.H. acknowledges the DURSI of Generalitat de Catalunya for financial support through Doctoral Fellowship 2005FI/00451. We are grateful to Dr. Pedro Salvador for useful comments in this work. The authors thank the Centre de Supercomputació de Catalunya (CESCA) for providing partial funding of computer time.

**Supporting Information Available:** Optimized Cartesian xyz coordinates of all stationary points located on the PES for each reaction mechanism studied in this work and the molecular orbital interaction diagram showing the comparison of coronene and anthanthrene derivatives coordinated to Cr(CO)<sub>3</sub>. This material is available free of charge via the Internet at <http://pubs.acs.org>.

#### References and Notes

- Deubzer, B.; Fritz, H. P.; Kreiter, C. G.; Ofele, K. *J. Organomet. Chem.* **1967**, *7*, 289–299. Muller, J.; Goser, P.; Elian, M. *Angew. Chem.-Int. Edit.* **1969**, *8*, 374–375; Oprunenko, Y. F. *Usp. Khim.* **2000**, *69*, 744–766. Dötz, K. H.; Wenzel, B.; Jahr, H. C. *Top. Curr. Chem.* **2004**, *248*, 63–103.
- Dötz, K. H.; Jahr, H. C. *Chem. Rec.* **2004**, *4*, 61–71.
- Hubig, S. M.; Lindeman, S. V.; Kochi, J. K. *Coord. Chem. Rev.* **2006**, *200–202*, 831–873.
- Albright, T. A.; Hofmann, P.; Hoffmann, R.; Lillya, C. P.; Dobosh, P. A. *J. Am. Chem. Soc.* **1983**, *105*, 3396–3411.
- Dötz, K. H.; Stinner, C.; Nieger, M. *J. Chem. Soc., Chem. Commun.* **1995**, 2535–2536. Oprunenko, Y. F.; Reshetova, M. D.; Malyugina, S. G.; Ustynyuk, Y. A.; Ustynyuk, N. A.; Batsanov, A. S.; Yanovsky, A. I.; Struchkov, Y. T. *Organometallics* **1994**, *13*, 2284–2290.
- Kirss, R. U.; Treichel, P. M. *J. Am. Chem. Soc.* **1986**, *108*, 853–855.
- Merlic, C. A.; Zechman, A. L.; Miller, M. M. *J. Am. Chem. Soc.* **2001**, *123*, 11101–11102.
- Arrais, A.; Diana, E.; Gervasio, G.; Gobetto, R.; Marabello, D.; Stanghellini, P. L. *Eur. J. Inorg. Chem.* **2004**, 1505–1513.
- Dötz, K. H.; Szesni, N.; Nieger, M.; Nattinen, K. J. *Organomet. Chem.* **2003**, *671*, 58–74. Longen, A.; Nieger, M.; Airola, K.; Dötz, K. H. *Organometallics* **1998**, *17*, 1538–1545.
- Oprunenko, Y. F.; Akhmedov, N. G.; Laikov, D. N.; Malyugina, S. G.; Mstislavsky, V. I.; Roznyatovsky, V. A.; Ustynyuk, Y. A.; Ustynyuk, N. A. *J. Organomet. Chem.* **1999**, *583*, 136–145.
- Pan, J.; Kampf, J. W.; Ashe, A. J. *Organometallics* **2006**, *25*, 197–202.
- Bradley, C. A.; Lobkovsky, E.; Keresztes, I.; Chirik, P. J. *J. Am. Chem. Soc.* **2005**, *127*, 10291–10304.
- Ochertyanova, E. A.; Hansen, H. J.; Ustynyuk, Y. A. *Helv. Chim. Acta* **2002**, *85*, 1166–1185.
- Jahr, H. C.; Nieger, M.; Dötz, K. H. *Chem. Commun.* **2003**, 2866–2867. Dötz, K. H.; Stinner, C.; Nieger, M. *J. Chem. Soc., Chem. Commun.* **1995**, 2535–2536.
- Jahr, H. C.; Nieger, M.; Dötz, K. H. *Chem.-Eur. J.* **2005**, *11*, 5333–5342.
- Dötz, K. H.; Stendel, J.; Müller, S.; Nieger, M.; Ketrat, S.; Dolg, M. *Organometallics* **2005**, *24*, 3219–3228.
- Tanabe, M.; Bourke, S. C.; Herbert, D. E.; Lough, A. L.; Manners, I. *Angew. Chem.-Int. Ed.* **2005**, *44*, 5886–5890.
- Own, Z. Y.; Wang, S. M.; Chung, J. F.; Miller, D. W.; Fu, P. P. *Inorg. Chem.* **1993**, *32*, 152–159.
- Mitchell, R. H.; Chen, Y. S.; Khalifa, N.; Zhou, P. Z. *J. Am. Chem. Soc.* **1998**, *120*, 1785–1794.
- Stoddart, M. W.; Brownie, J. H.; Baird, M. C.; Schmider, H. L. *J. Organomet. Chem.* **2005**, *690*, 3440–3450.



- (21) Güell, M.; Poater, J.; Luis, J. M.; M<sup>o</sup>, O.; Yáñez, M.; Solà, M. *ChemPhysChem* **2005**, *6*, 2552–2561.
- (22) Suresh, C. H.; Koga, N.; Gadre, S. R. *Organometallics* **2000**, *19*, 3008–3015.
- (23) Kündig, E. P.; Desobry, V.; Grivet, C.; Rudolph, B.; Spichiger, S. *Organometallics* **1987**, *6*, 1173–1180.
- (24) Mukerjee, S. L.; Lang, R. F.; Ju, T.; Kiss, G.; Hoff, C. D.; Nolan, S. P. *Inorg. Chem.* **1992**, *31*, 4885–4889.
- (25) Garg, A.; Nemer, D. M.; Choi, H. J.; Sheridan, J. B.; Geiger, W. E. *Organometallics* **2006**, *25*, 275–282. Jahr, H. C.; Nieger, M.; Dotz, K. H. *J. Organomet. Chem.* **2002**, *641*, 185–194. Oprunenko, Y.; Malyugina, S.; Nesterenko, P.; Mityuk, D.; Malyshev, O. *J. Organomet. Chem.* **2000**, *597*, 42–47. Oprunenko, Y.; Malyugina, S.; Vasil'ko, A.; Lyssenko, K.; Elschenbroich, C.; Harms, K. *J. Organomet. Chem.* **2002**, *641*, 208–214.
- (26) Oprunenko, Y.; Gloriov, I.; Lyssenko, K.; Malyugina, S.; Mityuk, D.; Mstislavsky, V.; Gunther, H.; von Firks, G.; Ebener, M. *J. Organomet. Chem.* **2002**, *656*, 27–42.
- (27) Howell, J. A. S.; Ashford, N. F.; Dixon, D. T.; Kola, J. C.; Albright, T. A.; Kang, S. K. *Organometallics* **1991**, *10*, 1852–1864.
- (28) Nunzi, F.; Mercuri, F.; De Angelis, F.; Sgamellotti, A.; Re, N.; Giannozzi, P. *J. Phys. Chem. B* **2004**, *108*, 5243–5249.
- (29) Ketrat, S.; Müller, S.; Dolg, M. *J. Phys. Chem. A* **2007**, *111*, 6094–6102.
- (30) Al-Takhin, G.; Connor, J. A.; Skinner, H. A.; Zafarani-Moattar, M. T. *J. Organomet. Chem.* **1984**, *260*, 189–197.
- (31) Alvarez, C. M.; Angelici, R. J.; Sygula, A.; Sygula, R.; Rabideau, P. W. *Organometallics* **2003**, *22*, 624–626.
- (32) Vecchi, P. A.; Alvarez, C. M.; Ellern, A.; Angelici, R. J.; Sygula, A.; Sygula, R.; Rabideau, P. W. *Organometallics* **2005**, *24*, 4543–4552.
- (33) Sygula, A.; Rabideau, P. W. *J. Chem. Soc., Chem. Commun.* **1994**, 2271–2272.
- (34) Mestres, J.; Solà, M. *J. Org. Chem.* **1998**, *63*, 7556–7558.
- (35) Haddon, R. C. *J. Comput. Chem.* **1998**, *19*, 139–143.
- (36) Mitchell, R. H. *Chem. Rev.* **2001**, *101*, 1301–1315. Mitchell, R. H.; Brikic, Z.; Berg, D. J.; Barclay, T. M. *J. Am. Chem. Soc.* **2002**, *124*, 11983–11988. Mitchell, R. H.; Zhou, P. Z.; Venugopalan, S.; Dingle, T. W. *J. Am. Chem. Soc.* **1990**, *112*, 7812–7813.
- (37) Schleyer, P. v. R.; Kiran, B.; Simion, D. V.; Sorensen, T. S. *J. Am. Chem. Soc.* **2000**, *122*, 510–513.
- (38) Simion, D. V.; Sorensen, T. S. *J. Am. Chem. Soc.* **1996**, *118*, 7345–7352.
- (39) Feixas, F.; Jimenez-Halla, J. O. C.; Matito, E.; Poater, J.; Solà, M. *Polish J. Chem.* **2007**, *81*, 783–797.
- (40) Frisch, M. J.; Trucks, G. W.; Schlegel, H. B.; Scuseria, G. E.; Robb, M. A.; Cheeseman, J. R.; Montgomery, J. A., Jr.; Vreven, T.; Kudin, K. N.; Burant, J. C.; Millam, J. M.; Iyengar, S. S.; Tomasi, J.; Barone, V.; Mennucci, B.; Cossi, M.; Scalmani, G.; Rega, N.; Petersson, G. A.; Nakatsuji, H.; Hada, M.; Ehara, M.; Toyota, K.; Fukuda, R.; Hasegawa, J.; Ishida, M.; Nakajima, T.; Honda, Y.; Kitao, O.; Nakai, H.; Klene, M.; Li, X.; Knox, J. E.; Hratchian, H. P.; Cross, J. B.; Adamo, C.; Jaramillo, J.; Gomperts, R.; Stratmann, R. E.; Yazyev, O.; Austin, A. J.; Cammi, R.; Pomelli, C.; Ochterski, J.; Ayala, P. Y.; Morokuma, K.; Voth, G. A.; Salvador, P.; Dannenberg, J. J.; Zakrzewski, V. G.; Dapprich, S.; Daniels, A. D.; Strain, M. C.; Farkas, O.; Malick, D. K.; Rabuck, A. D.; Raghavachari, K.; Foresman, J. B.; Ortiz, J. V.; Cui, Q.; Baboul, A. G.; Clifford, S.; Cioslowski, J.; Stefanov, B. B.; Liu, G.; Liashenko, A.; Piskorz, P.; Komaromi, I.; Martin, R. L.; Fox, D. J.; Keith, T.; Al-Laham, M.; Peng, C.; Nanayakkara, A.; Challacombe, M.; Gill, P. M. W.; Johnson, B. G.; Chen, W.; Wong, M. W.; González, C.; Pople, J. A. Gaussian 03, rev. B03; Gaussian Inc.: Pittsburgh, PA, 2003.
- (41) Becke, A. D. *J. Chem. Phys.* **1993**, *98*, 5648–5652.
- (42) Lee, C. T.; Yang, W. T.; Parr, R. G. *Phys. Rev. B* **1988**, *37*, 785–789.
- (43) Low, A. A.; Hall, M. B. *Int. J. Quantum Chem.* **2000**, *77*, 152–160.
- (44) Francl, M. M.; Pietro, W. J.; Hehre, W. J.; Binkley, J. S.; Gordon, M. S.; Defrees, D. J.; Pople, J. A. *J. Chem. Phys.* **1982**, *77*, 3654–3665. Hariharan, P. C.; Pople, J. A. *Theor. Chim. Acta* **1973**, *28*, 213–222.
- (45) Wachters, A. J. *J. Chem. Phys.* **1970**, *52*, 1033–1036.
- (46) Jacobsen, H.; Schreckenbach, G.; Ziegler, T. *J. Phys. Chem.* **1994**, *98*, 11406–11410.
- (47) Boys, S. F.; Bernardi, F. *Mol. Phys.* **1970**, *19*, 553–566. Salvador, P.; Duran, M. *J. Chem. Phys.* **1999**, *111*, 4460–4465.
- (48) Kruszewski, J.; Krygowski, T. M. *Tetrahedron Lett.* **1972**, *13*, 3839–3842. Krygowski, T. M. *J. Chem. Inf. Comput. Sci.* **1993**, *33*, 70–78.
- (49) Poater, J.; Duran, M.; Solà, M.; Silvi, B. *Chem. Rev.* **2005**, *105*, 3911–3947.
- (50) Fradera, X.; Austen, M. A.; Bader, R. F. W. *J. Phys. Chem. A* **1999**, *103*, 304–314. Fradera, X.; Poater, J.; Simon, S.; Duran, M.; Solà, M. *Theor. Chem. Acc.* **2002**, *108*, 214–224.
- (51) Bader, R. F. W. *Atoms in Molecules: A Quantum Theory*; Clarendon: Oxford, 1990.
- (52) Poater, J.; Fradera, X.; Duran, M.; Solà, M. *Chem. Eur. J.* **2003**, *9*, 400–406.
- (53) Matito, E.; Duran, M.; Solà, M. *J. Chem. Phys.* **2005**, *122*, 014109; Erratum **2006**, *125*, 059901.
- (54) Baerends, E. J.; Autschbach, J.; Bérces, A.; Bo, C.; de Boeij, P. L.; Boerrigter, P. M.; Cavallo, L.; Chong, D. P.; Deng, L.; Dickson, R. M.; Ellis, D. E.; Fan, L.; Fischer, L. H.; Fonseca Guerra, C.; van Gisbergen, S. J. A.; Groeneveld, J. A.; Gritsenko, O. V.; Grüning, M.; Harris, F. E.; van den Hoek, P.; Jacobsen, H.; Jensen, L.; van Kessel, G.; Kootstra, F.; van Lenthe, E.; McCormack, D. A.; Michalak, A.; Osinga, V. P.; Patchkovskii, S.; Philipsen, P. H. T.; Post, D.; Pye, C. C.; Ravenek, W.; Ros, P.; Schipper, P. R. T.; Schreckenbach, G.; Snijders, J. G.; Solà, M.; Swart, M.; Swerhone, D.; te Velde, G.; Vernooijs, P.; Versluis, L.; Visser, O.; Wang, F.; van Wezenbeek, E.; Wiesenecker, G.; Wolff, S. K.; Woo, T. K.; Yakovlev, A. L.; Ziegler, T. *ADF 2005*; Vrije Universiteit: Amsterdam, The Netherlands, 2005.
- (55) Ziegler, T.; Rauk, A. *Theor. Chim. Acta* **1977**, *46*, 1–10. Kitaura, K.; Morokuma, K. *Int. J. Quantum Chem.* **1976**, *10*, 325–340. Morokuma, K. *J. Chem. Phys.* **1971**, *55*, 1236–1244.
- (56) Becke, A. D. *Phys. Rev. A* **1988**, *38*, 3098–3100.
- (57) Snijders, J. G.; Baerends, E. J.; Vernooijs, P. *At. Nucl. Data Tables* **1982**, *26*, 483–509. Vernooijs, P.; Snijders, J. G.; Baerends, E. J. *Slater Type Basis Functions for the Whole Periodic System*; Vrije Universiteit: Amsterdam, The Netherlands, 1981.
- (58) Zhurko, G. A.; Zhurko, D. A. ChemCraft v. 1.5, <http://www.chemcraftprog.com>.
- (59) Kunz, V.; Nowacki, W. *Helv. Chim. Acta* **1967**, *50*, 1052–1059.
- (60) Bailey, M. F.; Dahl, L. F. *Inorg. Chem.* **1965**, *4*, 1314–1319. Rees, B.; Coppens, P. *Acta Cryst.* **1973**, *B29*, 2516–2528.
- (61) Brown, D. L. S.; Connor, J. A.; Demain, C. P.; Leung, M. L.; Martinho-Simoes, J. A.; Skinner, H. A.; Zafarani-Moattar, M. T. *J. Organomet. Chem.* **1977**, *142*, 321–335.
- (62) Baldrige, K. K.; Siegel, J. S. *J. Phys. Chem.* **1996**, *100*, 6111–6115. Ellass, A.; Mahieu, J.; Brocard, J.; Surpateanu, G.; Vergoten, G. *J. Mol. Struct.* **1999**, *475*, 261–272.
- (63) Seiders, T. J.; Baldrige, K. K.; O'Connor, J. M.; Siegel, J. S. *Chem. Commun.* **2004**, 950–951. Petrukhina, M. A.; Scott, L. T. *Dalton Trans.* **2005**, 2969–2975.
- (64) Haddon, R. C. *J. Am. Chem. Soc.* **1990**, *112*, 3385–3389.
- (65) Zhu, G.; Janak, K. E.; Figueroa, J. S.; Parkin, G. *J. Am. Chem. Soc.* **2006**, *128*, 5452–5461.
- (66) Calhorda, M. J.; Veiros, L. F. *Coord. Chem. Rev.* **1999**, *186*, 37–51. Veiros, L. F. *Organometallics* **2000**, *19*, 5549–5558.
- (67) The description of the MO in terms of fragment MO coefficients instead of Gross Mulliken contributions yields the same picture but it has the disadvantage of not being normalized, that is, the figures do not add up to 1 (or to 100%).